Catal Lett (2009) 130:227–234
DOI 10.1007/s10562-009-9870-9

Microwave-assisted Synthesis and Structural Characterization of Nanosized $Ce_{0.5}Zr_{0.5}O_2$ for CO Oxidation

Benjaram M. Reddy · Gunugunuri K. Reddy · Ibram Ganesh · Jose M. F. Ferreira

Received: 1 December 2008 / Accepted: 16 January 2009 / Published online: 4 February 2009

Abstract Nanosized $Ce_{0.5}Zr_{0.5}O_2$ solid solution has been synthesized by microwave-induced solution combustion method (MWCZ) and compared with that of a $Ce_xZr_{1-x}O_2$ solid solution with the same composition but prepared by the conventional coprecipitation method (CPCZ) and calcined at 773 K. X-ray diffraction and cell parameter studies revealed the incorporation of more zirconia and formation of more defect sites in the ceria lattice of the material prepared by microwave method. Raman spectroscopic measurements suggested the presence of oxygen vacancies, lattice defects and displacement of oxygen ions from their ideal lattice positions. X-ray photo electron spectroscopic studies indicated a high reducibility and surface enrichment of Ce^{3+} ions in the MWCZ sample. Better oxygen storage capacity and CO oxidation activity was observed for MWCZ in comparison to that of CPCZ sample. The significance of the microwave method lies mainly in its simplicity, flexibility, and easy control of different factors that determine the activity of the mixed oxide.

B. M. Reddy (✉) · G. K. Reddy
Inorganic and Physical Chemistry Division, Indian Institute of Chemical Technology (IICT), Uppal Road, Hyderabad 500607, India
e-mail: bmreddy@iict.res.in; mreddyb@yahoo.com

I. Ganesh (✉)
International Advanced Research Centre for Powder Metallurgy and New Materials (ARCI), Balapur (PO), Hyderabad 500005, India
e-mail: ibramganesh@arci.res.in; ibram_ganesh@yahoo.com

J. M. F. Ferreira
Department of Ceramics and Glass Engineering, CICECO, University of Aveiro, 3810193 Aveiro, Portugal

Keywords Microwave synthesis · Ceria–zirconia · Nano-oxides · Catalyst characterization · Raman spectroscopy · X-ray diffraction · CO oxidation

1 Introduction

In recent years, lots of nanomaterial-based catalysts have been investigated for catalytic oxidation of CO at low temperatures due to wide applications. Particularly, these applications include air-purification devices for respiratory protection, pollution control devices for reducing industrial and environmental emissions, removal of trace quantities of CO from the ambient air in closed atmospheres such as submarines and space crafts, exhaust abatement for CO_2 lasers, automotive emission control, and CO preferential oxidation for proton exchange membrane fuel cells [1]. Neutralization of gas emissions containing CO and toxic organic compounds by catalytic combustion is a widely used method based on the complete oxidation over suitable catalyst systems in the presence of oxygen or ozone [2–6]. Precious metals are well-known oxidation catalysts with high activity and stability, and are widely used for CO oxidation. However, due to high cost of precious metals and their sensitivity to sulphur poisoning, attention has been given to improve the catalytic performance of metal oxide catalysts.

In order to obtain a good oxide-based catalyst for CO oxidation, two ionic valence states must transpire with sufficient electrochemical potential (thermodynamic aspect), and also the switching between them must occur very promptly (kinetic aspect). Migration of oxygen on the surface of catalysts is most important in oxidation reactions where catalysts are subjected to repeated oxidation–reduction cycles [7]. Amongst all catalytically active oxides,

ceria (CeO_2) is quite apart due to its exceptional properties. During the last two decades ceria has been widely used as an active ingredient in automotive three-way catalysts (TWC) and also in electrochemical systems such as fuel cells [8]. Ceria, which has a fluorite type structure, is known to show large deviation from its CeO_2-stoichiometric composition. However, one of the major drawbacks of ceria is its poor resistance towards sintering. Ceria having a cubic related structure is known to sinter equally along the three *x, y* and *z* axes [9]. According to a rule established some years ago, sintering of oxides is favoured for metals having a high atomic weight, as is the case of cerium. There has been a lot of research to hinder or retard sintering by doping or mixing ceria with other oxides. Unlike the non-stoichiometric cerium oxide, the doped cerium oxide is stable in atmosphere and is often used as a solid-state electrolyte because it has enormous inborn oxygen vacancies and superior oxygen-ion conductivity. One of the main breakthroughs was the use of zirconia as a dopant [10]. ZrO_2 is a refractory oxide having the same fluorite (8:4) structure. Zr^{4+} ions enter the ceria network without too much stress and solid solutions of ceria–zirconia whatever the composition have been synthesized and used with success [11, 12]. This has been valuable for enhancing the thermal stability, the sintering resistance, oxygen storage capacity (OSC), electrochemical and catalytic properties [13, 14]. The origin of the enhanced reducibility and improved OSC may be due to several reasons including the presence of structural defects, which induce high mobility of bulk oxygen ions, even at moderate temperatures.

So far several preparative routes were employed to make ceria–zirconia solid solutions. Each method has its own advantages and disadvantages. Compared with conventional methods, microwave synthesis has the advantages of very short reaction times and production of small particles with narrow size distribution and high purity [15–17]. Because of its novel thermal heating mechanism, microwave energy heats the entire sample volume almost uniformly. The surface of sample radiates energy, resulting in high temperature at the interior of the sample [18]. The effect of heating is created by the interaction of the dipole moment of the molecules with the high frequency electromagnetic radiation. Water has a very high dipole moment which makes it one of the best solvents for microwave combustion synthesis [18, 19].

The primary objective of the present investigation was to explore the usefulness of microwave-solution combustion method to synthesize homogeneous $Ce_{0.5}Zr_{0.5}O_2$ solid solutions adopting the simple and cost effective processing route. For comparison purposes, an identical molar composition of $Ce_xZr_{1-x}O_2$ solid solution was also prepared by conventional coprecipitation method followed by calcination at 773 K. Samples obtained by both methods were characterized by means of X-ray diffraction, BET surface area, Raman spectroscopy, X-ray photoelectron spectroscopy, oxygen storage/release capacity measurements and eventually tested for their CO oxidation activity.

2 Experimental

2.1 Sample Preparation

To synthesize $Ce_xZr_{1-x}O_2$ (1:1 molar ratio based on oxides) solid solutions by microwave-induced solution combustion method, cerium and zirconyl nitrates were chosen as the precursors since nitrates favour combustion. In a typical experiment, the required quantities of cerium(III) nitrate (Aldrich, AR grade) and zirconyl(IV) nitrate (Fluka, AR grade) were dissolved separately in deionised water and mixed together in a Pyrex glass dish (150 mm diameter × 80 mm height). A stoichiometric quantity (as per the concept used in propellant chemistry) of solid urea (Fluka, AR grade) was added to the aforementioned mixture solution and stirred rigorously to obtain a clear solution. The dish containing the reaction mixture was introduced into a modified domestic microwave oven (BPL, India Limited, BMO-700T, 2.54 GHz, 700 W). Initially, the solution boils and undergoes dehydration followed by decomposition and spontaneous combustion with the evolution of large amounts of gases, including N_2, CO_2, and H_2O along with some traces of NH_3 and NO_2 followed by a spontaneous flame resulting in a light yellow residual mass. The entire process of liquid evaporation, thickening of the solution and combustion in the microwave oven took around 40 min to produce highly voluminous $Ce_xZr_{1-x}O_2$ powders. Three to four experiments were conducted under identical conditions to check for reproducibility. Properties of all the synthesized powders were found to be identical.

$Ce_xZr_{1-x}O_2$ (1:1 mole ratio) solid solution was also prepared by a coprecipitation method with dilute ammonium hydroxide (0.1 M). In a typical experiment, the required quantities of cerium(III) nitrate (Aldrich, AR grade) and zirconyl(IV) nitrate (Fluka, AR grade) were dissolved separately in deionised water and mixed together. Dilute liquid ammonia solution was added drop-wise to the mixture solution with vigorous stirring until the precipitation was complete. The resulting precipitate was filtered off, washed with deionised water, oven dried at 383 K for 16 h, and calcined at 773 K for 5 h in air atmosphere.

2.2 Characterization

The BET surface areas of the powders were determined by N_2 adsorption at liquid nitrogen temperature using a

Micromeritics Gemini 2360 instrument. Prior to analysis, samples were oven dried at 393 K for 12 h and flushed with Argon gas for 2 h. XRD patterns were recorded on a Bruker (Karlsruhe, Germany) D8 advanced system using a diffracted beam monochromated Cu Kα (0.15418 nm) radiation source. The intensity data were collected over a 2θ range of 3–80° with a 0.02° step size and using a counting time of 1 s per point. Crystalline phases were identified by comparison with the reference data from the International Centre for Diffraction Data (ICDD). The average crystallite size of the oxide phases was estimated employing Scherrer equation and considering the XRD data of all prominent lines [20]. The lattice parameters were calculated by a standard cubic indexation method using the intensity of the most prominent peak (111) [21]. The Raman spectra were recorded on a triple subtractive Jobin Yvon T64000 Raman spectrometer equipped with a liquid nitrogen-cooled charge-coupled device (CCD) detector. The emission line at 514.5 nm from the Ar^+ ion laser was focused on the sample under the microscope, with the width of the analyzed spot being about 1 μm. The power of the incident beam on the sample was about 5 mW. The XPS measurements were performed using a CEMUP-LAS (SECALAB 200A) spectrometer by using Mg Kα (1,253.6 eV) radiation as the excitation source. The charging of the powders was corrected by setting the binding energy of the adventitious carbon (C 1 s) at 284.6 eV. The XPS analysis was done at ambient temperature and at pressures typically below 10^{-6} Pa. Quantification of the atomic ratios was achieved by determining the elemental peak areas, following a Shirley background subtraction by the usual procedures documented in the literature [22].

2.3 Activity Measurements

The potential OSC was examined by oxygen release characteristics of the powders in the temperature range 573–1,073 K. The change in the weight of the sample was monitored by thermogravimetry (TG) under cyclic heat treatments in flowing nitrogen and dry air. A commercial Mettler Toledo TG-DTA analyzer was employed for this purpose. The heat cycle consisted of heating the sample to 1,073 K in N_2, cooling down to 423 K in dry air, and again heating to 1,073 K in N_2 environment. All heating and cooling rates were at 5 K min^{-1}. The weight loss of the sample during second heating cycle was used to measure the oxygen release properties [21]. CO oxidation was conducted in a fixed-bed microreactor under normal atmospheric pressure at 300–773 K under a heating ramp of 5 K min^{-1}. About 100 mg catalyst sample (250–355 μm sieve fraction) diluted with quartz particles of the same sieve fraction was placed in a quartz reactor for evaluation. The following gases and gas mixtures were used (supplied by Air Liquide): argon (>99.999% purity), 9.98% CO in argon (CO purity, >99.997%; argon purity, >99.99%), and 10.2% O_2 in argon (oxygen purity, >99.995%). The total flow rates maintained by three mass flow controllers were in the range of 50–100 NmL min^{-1} (millilitres normalized to 273.15 K and 1 atmosphere). The CO and CO_2 gas concentrations were measured using an Uras 14 infrared analyzer module, and the O_2 concentration was measured using a Magnos 16 analyzer (Hartmann & Braun). Prior to oxidation of CO, the catalysts were heated to 773 K in 10.2% O_2/Ar gas mixture, using a heating ramp of 10 K min^{-1}, and kept at the final temperature for 1 h. The oxidized sample was then purged in argon and cooled to the desired starting temperature. The CO/O_2 reactant feed ratio was 1, and partial pressures of CO and O_2 were in the range of 10 mbar [23].

3 Results and Discussion

The X-ray powder diffraction patterns of the two samples prepared in the present study are shown in Fig. 1. It can be seen that a cubic fluorite type solid solution with the composition $Ce_{0.5}Zr_{0.5}O_2$ (PDF-ICDD 38-1436) has been formed in the microwave-synthesized sample. However, the CPCZ sample prepared by coprecipitation and calcined at 773 K exhibited relatively poor crystallinity and only

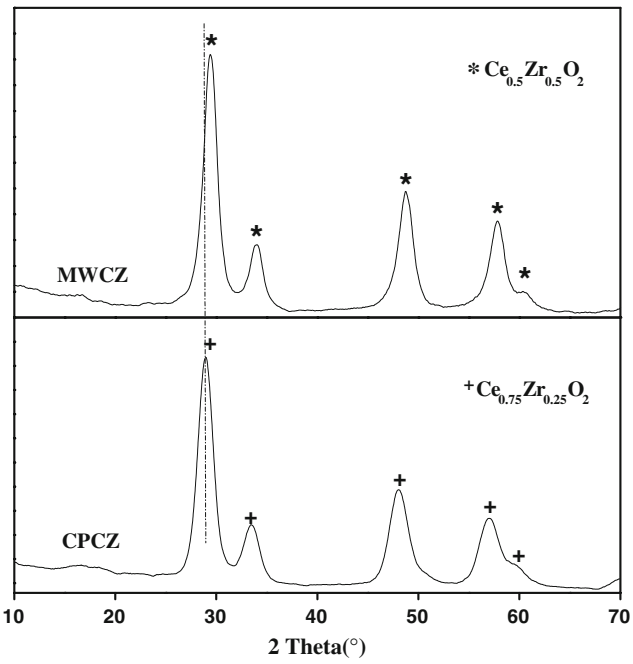

Fig. 1 X-ray powder diffraction patterns of $Ce_xZr_{1-x}O_2$ samples (*MWCZ* ceria–zirconia prepared by microwave method; *CPCZ* ceria–zirconia prepared by coprecipitation method)

broad diffraction lines due to cubic fluorite type phase with the composition $Ce_{0.75}Zr_{0.25}O_2$ (PDF-ICDD 28-0271) has been identified. Within the detection limits of XRD technique there is no evidence about the presence of t-ZrO_2 or m-ZrO_2 phases. It appears that the remaining zirconia is mostly in amorphous form probably segregated at the grain boundaries. Ceria crystallizes in a cubic fluorite structure and exposes the thermodynamically most stable (111) surface. This surface is the oxygen termination of the stoichiometric O–Ce–O tri layers stacked along the [111] direction and also represents a major fraction of the active surface in catalytic nanocrystallites [24]. Lattice parameter estimations provide information whether the foreign cations enter into the ceria lattice resulting in the formation of solid solutions or remain as separate phases demarcated by a phase boundary [21]. Using the most intense line (111) of the pattern, cubic indexation and calculation of unit cell parameters have been carried out and the values are presented in Table 1. The decrease in the cell parameter "*a*" of MWCZ sample (5.30 Å) compared to CPCZ sample (5.35 Å) is a clear indication of the incorporation of more Zr^{4+} cations into the ceria core fcc lattice (space group *Fm*3*m*) [25], which is in line with XRD results. The N_2 BET surface areas and OSC in terms of oxygen vacancy concentration pertaining to MWCZ and CPCZ samples are also presented in Table 1. MWCZ sample exhibits less surface area than CPCZ sample. This is due to the fact that, during the course of combustion synthesis the MWCZ sample is subjected to higher temperatures, however, for a limited period of time. It is suggested that the surface area may not be the only parameter that determines the catalytic efficiency of ceria because in pure ceria weakly bound active oxygen species are present in the bulk rather than on the surface [26, 27].

Raman spectra of both samples prepared in the present study are collected in Fig. 2. The samples MWCZ and CPCZ show strong bands at 470 and 468 cm^{-1}, respectively, and a less prominent broad band at 625 cm^{-1}, while a band at 300 cm^{-1} is detected only for the MWCZ sample. The band at 470 cm^{-1} can be attributed to the F_{2g} vibration of the fluorite type lattice [28]. It can be viewed as a symmetric breathing mode of the oxygen atoms around the cerium ions [29]. The slight shift in the Raman frequency to higher wave numbers in case of MWCZ sample could be due to incorporation of more zirconium into the ceria lattice compared to CPCZ, as evidenced by XRD results. As presented in Fig. 2, the peak at 470 cm^{-1} is more intense in case of MWCZ sample. It should be mentioned here that the intensity of the Raman band depends on several factors including grain size and morphology [30]. It is known that high temperature preparation conditions enhance the formation of oxygen vacancies, which perturb the local M–O bond symmetry leading to the relaxation of symmetry selection rules. The presence of a weak and less prominent broad band near 625 cm^{-1} can be attributed to a non-degenerate longitudinal optical (LO) mode of ceria arising due to relaxation of symmetry rules, which in turn is linked to oxygen vacancies in the ceria lattice [31–33]. In particular, the enhanced substitution of zirconium into the ceria lattice with an increase in temperature gives rise to oxygen vacancies, which are responsible for the emergence of this band [28]. This band is more intense in case of MWCZ sample, which indicates the incorporation of more zirconium into ceria lattice and formation of more oxygen vacancies in the MWCZ sample. The band at 300 cm^{-1} of MWCZ sample can be attributed

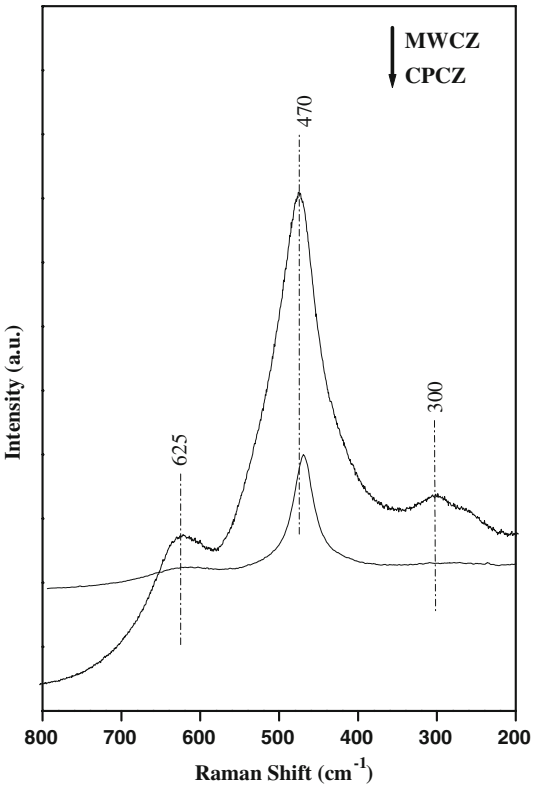

Fig. 2 Raman spectra of $Ce_xZr_{1-x}O_2$ samples (*MWCZ* ceria–zirconia prepared by microwave method; *CPCZ* ceria–zirconia prepared by coprecipitation method)

Table 1 BET surface area, crystallite size, cell parameter, and oxygen storage capacity values of $Ce_xZr_{1-x}O_2$ samples prepared by co precipitation (calcined at 773 K) and microwave combustion methods

$Ce_xZr_{1-x}O_2$ sample	BET surface area (m^2/g)	Crystallite size (nm)	Cell parameter (Å)	OSC μ moles O_2/g CeO_2–ZrO_2
Microwave method	56	12.7	5.3	278
Coprecipitation method	84	4.7	5.35	211

to displacement of oxygen atoms from their ideal fluorite lattice positions [34]. As per the literature reports, this band further reveals the presence of t″ phase, which could not be identified by XRD. The presence of this phase is expected to enhance the catalytic performance of this system [35, 36]. The presence of this band together with a high intensity band at 625 cm^{-1} clearly reflects the enhanced oxygen vacancy concentration in the MWCZ sample as determined by OSC measurements (Table 1).

Photoelectron spectroscopy has been used to obtain further information about the valence/oxidation state of the elements and surface composition of the Ce–Zr mixed oxides by inspecting the spectral line shapes and the intensities of the Ce 3d core level electrons. Figure 3 compares the Ce 3d spectra of the ceria–zirconia solid solutions prepared by two different methods. The binding energy values are presented in Table 2. The bands labelled v collectively represent the Ce $3d_{5/2}$ ionization, while bands labelled u represent the Ce $3d_{3/2}$ ionization [37]. The bands with unprimed labels represent the primary Ce $3d_{5/2}$ and Ce $3d_{3/2}$ transitions, while the primed labels represent ionization satellite features. Specifically, the band (u_0, u) is the Ce $3d_{3/2}$ ionization and the band (v_0, v) is the Ce $3d_{5/2}$ ionization for Ce^{3+} and Ce^{4+}. The bands labelled v′, v″, v‴ and u′, u″, u‴ are satellites arising from the Ce $3d_{5/2}$ ionization and Ce $3d_{3/2}$ ionization, respectively [38–40]. The observed binding energy values presented in Table 2 are in good agreement with those reported in the literature [41]. The shift in the binding energy to higher values in case of microwave-synthesized sample may be due to better reducibility of the sample. The Ce/Zr atomic ratios presented in the Table 2 clearly indicate that the sample prepared by microwave method has a more extended incorporation of zirconium into the ceria lattice in comparison to the sample prepared by coprecipitation method, corroborating with the XRD and Raman spectroscopic results. In Fig. 3, the peaks labelled u_0, u′, v_0, and v′ correspond to Ce^{3+} oxidation state and the remaining peaks correspond to Ce^{4+} oxidation state. Generally, the Ce^{3+} content (reducibility) is determined by calculating the area under the peaks u_0, u′, v_0, and v′. But the v_0 line appears as a shoulder in the main v contribution, thus being difficult to

Table 2 XPS data obtained for the $Ce_xZr_{1-x}O_2$ samples prepared by co precipitation (calcined at 773 K) and microwave combustion methods

$Ce_xZr_{1-x}O_2$ sample	Ce $3d_{5/2}$	Zr $3d_{5/2}$	O 1 s	U‴ (%)	Ce/Zr atomic ratio
Microwave method	882.7	182.3	530.3	7	3.46
Coprecipitation method	882.5	182.2	530.1	9.5	4.04

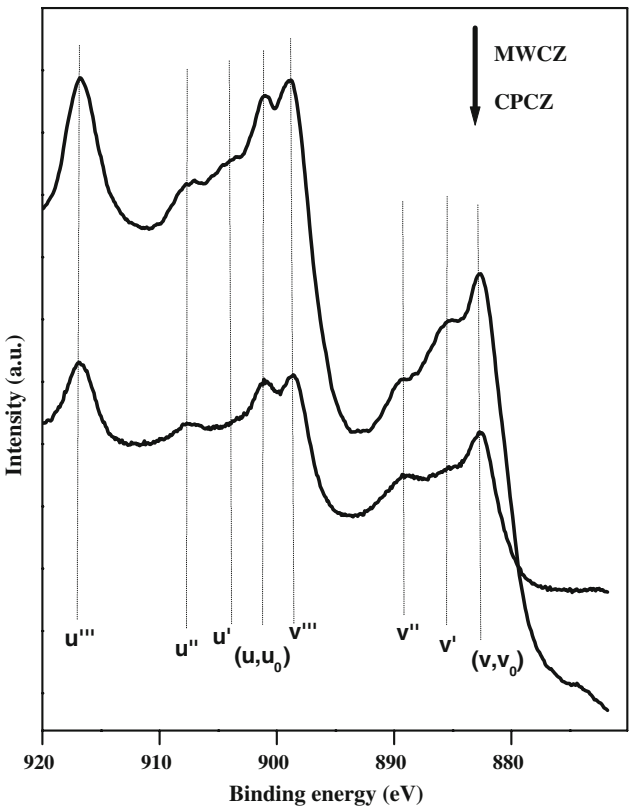

Fig. 3 Ce 3d XPS spectra of $Ce_xZr_{1-x}O_2$ samples (*MWCZ* ceria–zirconia prepared by microwave method; *CPCZ* ceria–zirconia prepared by coprecipitation method)

detect. The u_0 line cannot be detected directly and is thus estimated from the intensity of v_0 [42]. Therefore, the % of intensity of u‴ peak to the total area was used to determine the surface concentration of Ce^{3+} or reducibility of the mixed oxide in the literature [43, 44]. The % of intensity values of u‴ peaks of the two samples prepared in the present study are presented in Table 2. Interestingly, both the mixed oxides exhibit relatively small intensity compared to pure ceria (14%), suggesting that both the materials contain Ce^{3+} ions in some reasonable quantities [43, 44]. The values presented in Table 2 clearly suggest an enhanced reducibility and a more extended surface enrichment of Ce^{3+} ions for the MWCZ sample.

As presented in Fig. 4a, the O 1 s peak is generally broad and complicated, because of the non-equivalence of surface O ions. As per the literature, the O ions in pure CeO_2 exhibit intense peaks at 528.6, 528.8, 529.6, and 530.1 eV [45–48], respectively. The O 1 s binding energy value reported for ZrO_2 is 530.6 eV [22]. The O 1 s binding energies pertaining to CPCZ and MWCZ samples are observed at 530.1, and 530.3, respectively. The broadening of the peak and slight increase in the binding energy in the case of MWCZ sample can be taken as an evidence for incorporation of zirconium into the CeO_2 lattice. As shown in Table 2 and Fig. 4b, the binding energy of the Zr 3d photoelectron peak

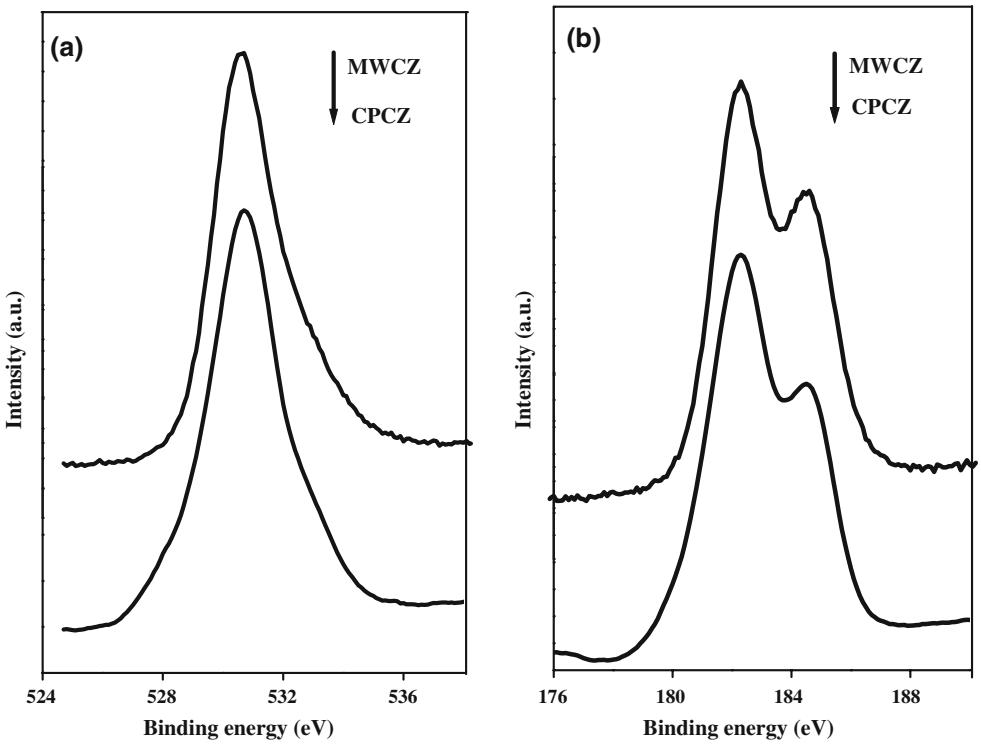

Fig. 4 XPS spectra of $Ce_xZr_{1-x}O_2$ samples **a** O 1 s, **b** Zr $3d_{5/2}$ (*MWCZ* ceria–zirconia prepared by microwave method; *CPCZ* ceria–zirconia prepared by coprecipitation method)

ranged between 182.2 and 182.6 eV, which agrees well with the values reported in the literature [49]. The core level spectra of Zr 3d in case of the MWCZ sample showed a slight broadening along with a small shift towards higher binding energy, indicating the incorporation of more zirconium into the ceria lattice.

The potential OSC of both the mixed oxides were evaluated by thermogravimetry. The oxygen vacancy concentration pertaining to these two samples are shown in Table 1. It can be noted that the MWCZ sample exhibits more OSC than CPCZ sample. The difference in OSC may be due to better reducibility of the MWCZ sample owing to more incorporation of zirconium that has led to higher defective sites. The presence of Raman band at 300 cm^{-1} and another intense band at 625 cm^{-1} also supports this observation. The CO oxidation results of MWCZ and CPCZ samples as a function of reaction temperature are shown in Fig. 5. Catalytic oxidation is known to be influenced by mass transfer at high conversions, and comparison of activity was made in terms of "light-off" temperature. Note that light-off means a jump of the activity to over 50% conversion very quickly, and this characteristic is very important for automobile emission control. As can be noted from Fig. 5, the MWCZ sample exhibits more CO conversion than CPCZ even at lower temperatures. The MWCZ sample reaches a light-off (50% conversion) temperature 44 K lower than that of the CPCZ sample. Furthermore, the MWCZ sample exhibited 100% CO conversion at 750 K, whereas the CPCZ showed 85% conversion at 773 K, the highest temperature investigated. It is generally accepted that CO oxidation under stationary conditions occurs over pure ceria by a Mars–van Krevelen-type mechanism, where the reaction involves alternate reduction and oxidation of the surface with the formation of surface oxygen vacancies (as the key step) and their successive replenishment by gas-phase oxygen [50, 51]. During the course of catalytic CO oxidation, one has to activate either of the reactants and this

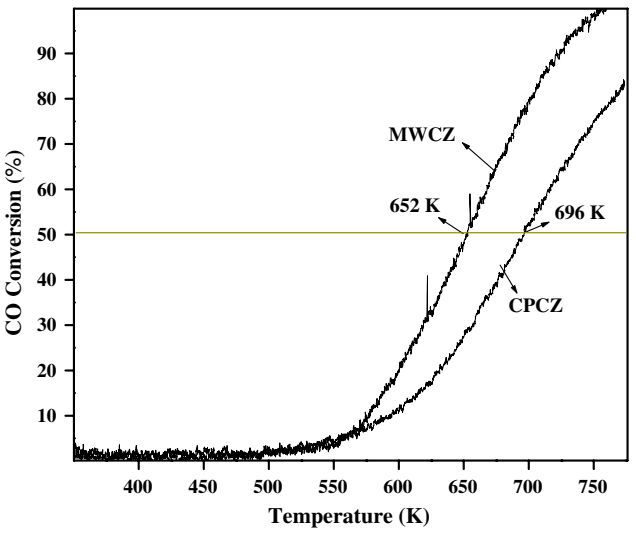

Fig. 5 Conversion of CO versus temperature profiles of $Ce_xZr_{1-x}O_2$ samples (*MWCZ* ceria–zirconia prepared by microwave method; *CPCZ* ceria–zirconia prepared by coprecipitation method)

occurs preferentially with oxygen. Thus in catalytic CO oxidation molecular oxygen is generally dissociated into radicals, which are strong oxidizers as well as strong electrophiles. From these observations, we may conclude that the higher is the OSC of the catalyst, the better will be the activity for CO oxidation. More than the total OSC, the local concentration of sites for O_2 adsorption would be a determining factor in CO oxidation. A close correlation between OSC and catalytic activity may, however, be found since a high concentration in anionic vacancy is a prerequisite for a high OSC value of the sample. The higher conversion and higher reducibility observed for the MWCZ sample could be due to the enhanced oxygen mobility in the defective fluorite structure generated by introduction of more Zr^{4+} cations into the ceria core lattice in comparison to the CPCZ sample.

4 Conclusions

Nanostructured homogeneous $Ce_{0.5}Zr_{0.5}O_2$ solid solution has been synthesized by adopting a simple and cost effective single step microwave-induced combustion process. The $Ce_xZr_{1-x}O_2$ solid solution with the same composition was also synthesized by a coprecipitation method and calcined at 773 K for comparison purpose. The results of XRD and cell parameter revealed that more zirconia was incorporated into the ceria lattice and higher defective sites were formed in the case of microwave-synthesized sample. The XPS results enable concluding that MWCZ exhibits higher reducibility and surface enrichment of Ce^{3+} ions. Raman and OSC measurements established that oxygen vacancies were more abundant in the sample prepared by microwave method. CO oxidation results showed that MWCZ sample exhibits lower light-off temperature as well as higher CO conversion (100%) compared to that of CPCZ sample under an identical set of experimental conditions. Higher reducibility, better OSC, and formation of higher defect sites in its crystal lattice due to incorporation of more zirconia are considered responsible for the better activity observed for MWCZ sample. In summary, it can be concluded that the synthesis of $Ce_xZr_{1-x}O_2$ solid solution by microwave-induced solution combustion method is a cost effective technique for low temperature CO oxidation in comparison to coprecipitation route.

Acknowledgments GKR thank UGC, New Delhi for senior research fellowship. The support of CICECO is acknowledged.

References

1. Min K, Song MW, Lee CH (2003) Appl Catal A Gen 251: 143–156
2. Song KS, Klvana D, Kirchnerova J (2001) Appl Catal A Gen 213:113–121
3. Zamostny P, Belohlav Z (2002) Appl Catal A Gen 225:291–299
4. Baldi M, Finocchio E, Milella F, Busca G (1998) Appl Catal B Environ 16:43–51
5. Burgos N, Paulis M, Antxustegi MM, Montes M (2002) Appl Catal B Environ 38:251–258
6. Naydenov A, Stoyanova R, Mehandjiev D (1995) J Mol Catal 98:9–14
7. Martinez-Arias A, Fernandez-Garcia M, Galvez O, Coronado JM, Anderson JA, Conesa JC, Soria J, Munuera G (2000) J Catal 195:207–216
8. Trovarelli A (2002) Catalysis by ceria and related materials In: Hutchings GJ (Series Editor), Catalytic Science Series, Vol. 2, Imperial College Press, London
9. Schmieg SJ, Belton DN (1995) Appl Catal B Environ 6:127–144
10. Kaspar J, Fornasiero P, Graziani M (1999) Catal Today 50:285–298
11. Fornasiero P, Di Monte R, Rao GR, Kaspar J, Meriani S, Trovarelli A, Graziani M (1995) J Catal 151:168–177
12. Trovarelli A, Leitenburg C, Dolcetti G (1997) Chem Tech 27:32–37
13. Rossignol S, Madier Y, Duprez D (1999) Catal Today 50:261–270
14. Colon G, Pijolat M, Valdivieso F, Vidal H, Kaspar J, Finocchio E, Daturi M, Binet C, Lavalley JC, Baker RT, Bernal S (1998) J Chem Soc Faraday Trans 94:3717–3726
15. Mingos DMP, Baghurst DR (1991) Chem Soc Rev 20:1–47
16. Fu Y-P, Lin C-H (2003) J Alloys Compds 354:232–235
17. Ganesh I, Johnson R, Mahajan YR, Madhavendra SS, Reddy BM (2005) Ceram Inter 31:67–74
18. Clark DE, Amad I, Dalton RC (1991) Mat Sci Eng A 144:91–97
19. Ganesh I, Johnson R, Mahajan YR, Khan A, Madhavendra SS, Reddy BM (2004) J Mater Res 19:1015–1023
20. Klug HP, Alexander LE (1974) X-ray diffraction procedures for polycrystalline and amorphous materials, 2nd edn. Wiley, New York
21. Reddy BM, Khan A (2005) Catal Surv Asia 9:155–171
22. Wagner CD, Riggs WM, Davis LE, Moulder JF (1978) In: Muilenberg GE (ed) Handbook of X-ray photoelectron spectroscopy. Perkin–Elmer Corporation, Minnesota
23. Reddy BM, Lakshmanan P, Bharali P, Saikia P, Thrimurthulu G, Muhler M, Gruenert W (2007) J Phys Chem C 111:10478–10483
24. Esch F, Fabris S, Zhou L, Montini T, Africh C, Fornasiero P, Comelli G, Rosei R (2005) Science 309:752–755
25. Meriani S, Spinolo G (1987) Powder Diffr 2:255–256
26. Bernal S, Kaspar J, Trovarelli A (1999) Catal Today 50:173–186 (Special Issue)
27. Putna ES, Vohs JM, Gorte RJ (1996) J Phys Chem 100:17862–17865
28. McBride JR, Hass KC, Poindexter BD, Weber WH (1994) J Appl Phys 76:2435–2441
29. Lin X–M, Li L-P, Li G-S, Su W-H (2001) Mater Chem Phys 69:236–240
30. Spanier JE, Robinson RD, Zhang F, Chan S-W, Herman IP (2001) Phys Rev B 64:245407.1–245407.8
31. Reddy BM, Khan A, Yamada Y, Kobayashi T, Loridant S, Volta JC (2003) Langmuir 19:3025–3030
32. Weber WH, Hass KC, McBride JR (1993) Phys ReV B 48: 178–185
33. Reddy BM, Lakshmanan P, Khan A, Loridant S, Cartes CL, Rojas TC, Fernandez AJ (2005) J Phys Chem B 109:13545–13552
34. Escribano VS, Lopez EF, Panizza M, Resini C, Amores JMG, Busca G (2003) Solid State Sci 5:1369–1376

35. Vlaic G, Fornasiero P, Geremia S, Kaspar J, Graziani M (1997) J Catal 168:386–392
36. Yashima M, Arashi H, Kakihana M, Yoshimura M (1994) J Am Ceram Soc 77:1067–1071
37. Rango R, Kaspar G, Meriani S, di Monte R, Graziani M (1994) Catal Lett 24:107–112
38. Burroughs P, Hamnett A, Orchard A, Thornton G (1976) J Chem Soc Dalton Trans 1686–1698
39. Albero JS, Reinoso FR, Escribano AS (2002) J Catal 210: 127–136
40. Barr TL, Fries CE, Cariati F, Bart JCJ, Giordano N (1983) J Chem Soc Dalton Trans 1825–1829
41. Bensalem A, Bozon-Verduraz F, Delamar M, Bugli G (1995) Appl Catal A Gen 121:81–93
42. Fallah JE, Hilaire L, Romeo M, Le Normand F (1995) J Electron Spectrosc Relat Phenom 73:89–103
43. Schmitz PJ, Usman RK, Peters CR, Graham CW, McCabe RW (1993) Appl Surf Sci 72:181–187
44. Martnez-Arias A, Fernandez-Garca M, Ballesteros V, Salamanca LN, Conesa JC, Otero C, Soria J (1999) Langmuir 15:4796–4802
45. Paparazzo E, Ingo GM, Zacchetti NJ (1991) J Vac Sci Technol A 9:1416–1420
46. Praline G, Koel BE, Hance RL, Lee H-I, White JM (1980) J Electron Spectrosc Relat Phenom 21:17–30
47. Pfau A, Schierbaum KD (1994) Surf Sci 321:71–80
48. Galtayries A, Sporken R, Riga J, Blanchard G, Caudano R (1998) J Electron Spectrosc Relat Phenom 88:951–956
49. Briggs D, Seah MP (1990) Practical surface analysis, auger and X-ray photoelectron spectroscopy, vol 1, 2nd edn. Wiley, New York
50. Boaro M, Vicario M, de Leitenburg C, Dolcetti G, Trovarelli A (2003) Catal Today 77:407–417
51. Assmann J, Narkhede V, Khodeir L, Loffler E, Hinrichsen O, Birkner A, Over H, Muhler M (2004) J Phys Chem B 108:14634–14642